

Optimizing nanoporous materials for gas storage

Electronic Supplementary Information (ESI)

Cory M. Simon^{*a}, Jihan Kim^b, Li-Chiang Lin^a, Richard L. Martin^c, Maciej Haranczyk^c,
and Berend Smit^a

^a University of California, Berkeley. Department of Chemical and Biomolecular Engineering.

^b Department of Chemical and Biomolecular Engineering, Korea Advanced Institute of Science and Technology, 291
Daehak-ro Yuseong-gu Daejeon, Korea 305-701

^c Lawrence Berkeley National Laboratory

*E-mail: CoryMSimon@gmail.com

Contents

S1 Molecular simulation details	S2
S2 A review of the force field used in the simulations	S2
S3 Obtaining geometric parameters	S2
S4 Model 0 details	S3
S4.1 Derivation	S3
S4.1.1 Approach 1	S4
S4.1.2 Approach 2	S5
S4.2 The universal fractional deliverable capacity vs energy of adsorption curve	S5
S4.3 Equivalence of $U_{0,opt}$ to Bhatia and Myers	S6
S4.4 The density of sites M is important	S6
S5 Model 1 details	S6
S5.1 Derivation	S6
S5.2 Asymptotic Expansion	S8
S5.3 How unfavorable guest-guest interactions may enhance a material's deliverable capacity	S8
S6 Model 2 details	S9
S6.1 Computing the standard entropy change	S9
S6.2 More detailed description of the model	S9
S6.3 Barrier to observed entropy change	S9
S7 Model 3: Spatially inhomogeneous adsorption site	S10
S7.1 Model 3 derivation	S11
S8 Fitting Isotherm data to a Langmuir model	S11
S9 Software	S12
S10 Discourse on ARPA-E target conditions	S12
S11 Distributions of properties in the zeolite data base	S13
S12 Other plots of data from the zeolite database	S15

S1 Molecular simulation details

The adsorption data, heat of adsorption, and void fraction for all hypothetical zeolite structures are obtained using our graphics processing units (GPU) code. The details behind the GPU algorithm are described elsewhere [1]. The energy grid that stores the guest-host and the guest-guest pair-wise interactions are constructed with a grid size of 0.15 Angstroms. For the Grand-canonical Monte Carlo simulations, the number of equilibration and production cycles is set to be 1 million and 1.6 million cycles, respectively. The void fraction values were obtained from the GPU routine that computes the methane Henry coefficient. Specifically, in the particle Widom insertion method, the total number of randomized methane insertion configurations is set to be $N_{\text{Widom}} = 35.84$ million. Out of N_{Widom} , we count the number of test points $N_{\text{Low energy}}$ where the methane-zeolite framework interaction energy is smaller than $\langle U \rangle + RT$, with $\langle U \rangle$ being the Boltzmann-weighted average energy of the system. The void fraction is then

$$\epsilon = \frac{N_{\text{Low energy}}}{N_{\text{Widom}}}. \quad (\text{S1})$$

The Henry coefficient K_H is computed by Widom insertions [2] and the expression

$$K_H = \beta \langle e^{-\beta U} \rangle. \quad (\text{S2})$$

For the isotherm data throughout the paper, the average of two simulations was used.

S2 A review of the force field used in the simulations

Here, we provide a brief validation of the reliability of the force field used to describe the interactions between methane and the solid zeolites atoms in this work. We used the force field developed in works [3,4], which was specifically tuned to reproduce adsorption isotherms of methane and other alkanes in zeolites. Figs S1(a) and (b) show that the force field reproduces the methane adsorption isotherms in MFI and an AFI-topology zeolite. In addition, Fig S1(c) shows that molecular simulations using the force field can reproduce experimental measurements of the diffusion coefficient of methane as a function of loading in MFI. Two reviews describing how these simulations have been used to increase our understanding of adsorbates in zeolites are in Refs. [5,6].

S3 Obtaining geometric parameters

Our open source porous materials analysis suite, Zeo++ [11], enables the rapid and high-throughput calculation of geometric properties and descriptors for all classes of porous materials. Zeo++ utilizes the Voronoi decomposition to construct a three-dimensional, periodic graph spanning the pore space inside a material. Briefly, the vertices of this graph correspond to the centers of local cavities in the structure (positions equidistant between four framework atoms), and the edges between vertices correspond to the direct pathways between these positions (equidistant between three framework atoms). This graph can be inspected to identify common material descriptors such as the diameter of the largest included sphere, corresponding to the largest spherical cavity inside a material. Furthermore, by utilizing a variant on the Dijkstra shortest path algorithm, paths traversing the material, corresponding to channel systems, can be identified with respect to a given probe radius. By exploiting this knowledge, the other descriptors utilized in this work, such as accessible surface area, can be efficiently computed through Monte Carlo sampling on only the probe-accessible regions of the structure. The algorithms for calculation of these and further descriptors are provided in detail in [11].

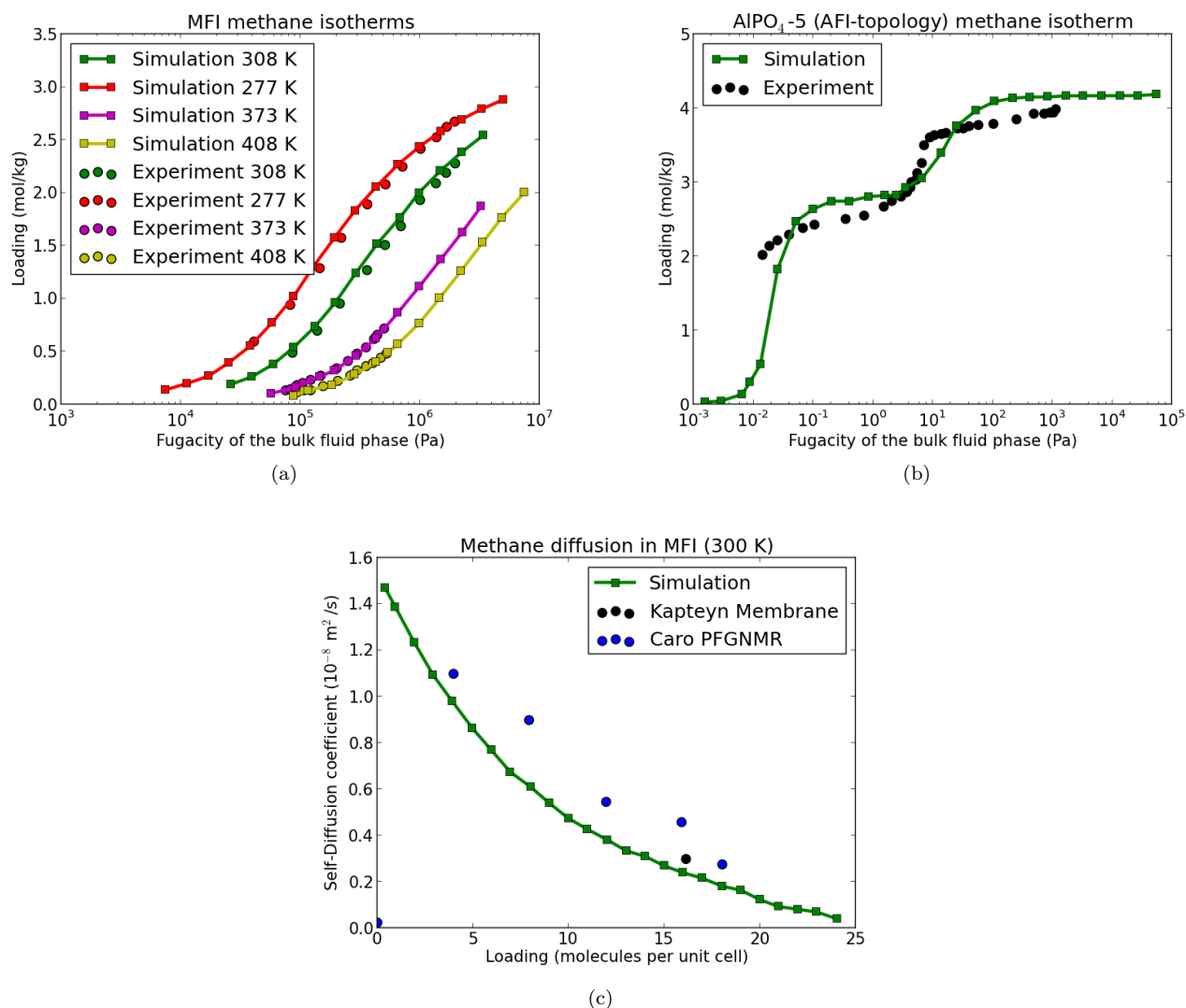


Figure S1. The force field [3] used in this work reproduces methane adsorption isotherms in (a) MFI (b) AlPO₄-5 (AFI-topology) zeolites. MFI experimental data is from [7, 8]. AlPO₄-5 experimental data is from [9]. (c) The same force field in [3] was later used to simulate the diffusion of methane in MFI as a function of loading in Ref [10]. The molecular simulations agree remarkably well with the data. Figs (a) and (b) were reproduced from Ref. [3] and (c) from Ref. [10] using Plot Digitizer.

S4 Model 0 details

S4.1 Derivation

Consider a gaseous phase of methane in equilibrium with an adsorbed phase of methane in a volume V of our model nanoporous material. Our goal here is to find the isotherm, i.e. the loading as a function of pressure (related to chemical potential).

S4.1.1 Approach 1

The condition for equilibrium between the adsorbed phase (*ads*) and the ideal gas phase (*ig*) is the equality of the chemical potential in the two phases:

$$\mu_{ads} = \mu_{ig}. \quad (\text{S3})$$

We obtain both μ_{ads} and μ_{ig} using the identity that relates the chemical potential to the Canonical partition function Q :

$$\mu = \left(\frac{\partial A}{\partial \sigma} \right)_{T,V} = -\frac{1}{\beta} \left(\frac{\partial \ln Q}{\partial \sigma} \right)_{T,V}. \quad (\text{S4})$$

When considering the adsorbed phase, M plays the role of volume. Our approach is to find the Canonical partition function for an ideal gas Q_{ig} and for the adsorbed phase Q_{ads} , perform the derivative in eqn S4, and equate the two chemical potentials.

The ideal gas. The single-particle partition function is generally:

$$q(V, T) = \frac{1}{\Lambda^3} \int_{\Omega} e^{-\beta U(x)} dx, \quad (\text{S5})$$

where Ω represents the system volume and $\Lambda = \Lambda(T)$ is the thermal de Broglie wavelength. Because ideal methane molecules do not interact, $U(x) = 0$ and we arrive at $q(V, T) = V/\Lambda^3$. Because ideal gas particles behave independently of one another, the Canonical partition function for an entire system of σ ideal gas particles is:

$$Q_{ig}(\sigma, V, T) = \frac{q(V, T)^\sigma}{\sigma!}, \quad (\text{S6})$$

where the factorial term takes into account that the particles are indistinguishable. Using Stirling's approximation for the factorial term and the identity in eqn S4, we take the derivative of Q_{ig} to arrive at the chemical potential for an ideal gas:

$$\mu_{ig} = \frac{1}{\beta} \ln(\Lambda^3 \rho), \quad (\text{S7})$$

where ρ is the density of the ideal gas.

The adsorbed phase. The Canonical partition function q of a single guest particle in a single adsorption site of our model material, considered the unit cell Ω in Fig 3, is found by using eqn S5 and the energy landscape in eqn 1:

$$q = \frac{1}{\Lambda^3} \epsilon \frac{V}{M} e^{-\beta U_0}, \quad (\text{S8})$$

since the volume of the unit cell is the total macroscopic volume V under consideration divided by the number of sites in that volume, M . The void fraction ϵ is the ratio of the volume of the binding pocket Ω_s to the volume of the entire unit cell Ω . Since the particles do not interact, the Canonical partition function $Q(\sigma, M, T)$ for σ molecules adsorbed onto a solid with M sites is then:

$$Q(\sigma, M, T) = \frac{M!}{\sigma!(M-\sigma)!} q^\sigma. \quad (\text{S9})$$

The binomial term $\binom{M}{\sigma}$ counts the number of arrangements of the σ molecules among the M sites. Using Stirling's formula for the $\binom{M}{\sigma}$ term and taking the derivative as in eqn S4, we arrive at the chemical potential for the adsorbed phase:

$$\mu_{ads} = -\frac{1}{\beta} \ln \left(\frac{M-\sigma}{\sigma} \frac{1}{\Lambda^3} \epsilon \frac{V}{M} e^{-\beta U_0} \right). \quad (\text{S10})$$

Finally, we equate the chemical potentials due to the equilibrium condition in eqn S3 and solve for the number of occupied sites σ :

$$\sigma = \frac{\beta \epsilon V e^{-\beta U_0} P}{1 + \frac{\beta \epsilon V e^{-\beta U_0}}{M} P}, \quad (\text{S11})$$

where we used the ideal gas law to relate the density to the pressure via $\rho = P\beta$. Since $\frac{\beta\epsilon V e^{-\beta U_0}}{M}$ is constant with temperature, we define it as a constant K to get the familiar Langmuir isotherm for fractional occupancy:

$$\frac{\sigma}{M} = \frac{KP}{1 + KP}. \quad (\text{S12})$$

S4.1.2 Approach 2

In the second approach, we directly find the average number of particles in the adsorbed phase when the particle number is allowed to fluctuate in the Grand-canonical ensemble. The Grand-canonical partition function under the equilibrium condition $\mu = \mu_{ig} = \mu_{ads}$ is:

$$\Xi(\mu, M, T) = \sum_{\sigma=0}^M Q(\sigma, M, T) e^{\beta\mu\sigma}. \quad (\text{S13})$$

We seek to derive the Langmuir isotherm by finding the average σ :

$$\langle\sigma\rangle = \sum_{n=0}^M nP(N=n) = \frac{1}{\Xi} \sum_{n=0}^M n e^{-\beta n U_0} e^{\beta\mu n} = \frac{\partial \ln \Xi}{\partial(\beta\mu)}. \quad (\text{S14})$$

First, we use eqn S9 to write the Grand Canonical partition function in eqn S13 as:

$$\Xi(\mu, M, T) = \sum_{\sigma=0}^M \binom{M}{\sigma} \left[\frac{\epsilon V}{M\Lambda^3} e^{-\beta U_0} e^{\beta\mu} \right]^\sigma, \quad (\text{S15})$$

which is a binomial expansion of the function $(1 + \frac{\epsilon V}{M\Lambda^3} e^{-\beta U_0} e^{\beta\mu})^M$. Taking the logarithm and performing the derivative in eqn S14:

$$\langle\sigma\rangle = \frac{\epsilon V e^{-\beta U_0} e^{\beta\mu}}{\Lambda^3 + \frac{\epsilon V e^{-\beta U_0}}{M} e^{\beta\mu}}. \quad (\text{S16})$$

Using the ideal gas law and the expression for the chemical potential of the bulk gas in equilibrium with the solid in eqn S7, we write this as:

$$\langle\sigma\rangle = \frac{\beta\epsilon V e^{-\beta U_0} P}{1 + \frac{\beta\epsilon V e^{-\beta U_0}}{M} P}, \quad (\text{S17})$$

which is equivalent to eqn S11 and therefore eqn. S12 in Approach 1, and we arrive at the Langmuir isotherm.

S4.2 The universal fractional deliverable capacity vs energy of adsorption curve

Using the definition of the effective heat of adsorption U^* in eqn 8, we substitute:

$$U_0 = U^* + RT \ln \left(\beta \frac{\epsilon}{M} \right), \quad (\text{S18})$$

into eqn S3 to get:

$$\frac{D}{M} = \frac{e^{-\beta U^*} P_2}{1 + e^{-\beta U^*} P_2} - \frac{e^{-\beta U^*} P_1}{1 + e^{-\beta U^*} P_1}, \quad (\text{S19})$$

This theoretical curve of $\frac{D}{M}$ depends only upon the effective heat of adsorption, and not the volume of the adsorption pocket in the material. It is plotted in Fig 4 as the black line.

S4.3 Equivalence of $U_{0,opt}$ to Bhatia and Myers

Here, we show that the eqn derived in [12] for the optimum heat of adsorption:¹,

$$\Delta H_{BM} = \frac{RT}{2} \log \left(\frac{P_L P_H}{(P^\circ)^2} \right) + T \Delta S^\circ, \quad (\text{S20})$$

for a Langmuirian material is consistent with eqn 4 for our model material in model 0 by applying eqn 20 to the model material in model 0. The term ΔS° is the standard entropy change upon adsorption with reference pressure $P^\circ = 1$ bar. The details of the reference state are in [13], briefly, “The reference states for the standard entropy of adsorption are a hypothetical perfect gas at one atmosphere for the gas phase and a hypothetical gas in the nanopores which obeys Henry’s law exactly”. In [13], it is show that ΔS° can be written:

$$\Delta S^\circ = \frac{\Delta H}{T} + R \ln \left(\frac{K_H P^\circ}{M} \right), \quad (\text{S21})$$

where K_H is Henry’s constant and M is the saturation loading. For model 0:

$$K_H = \beta \epsilon e^{-\beta U_0} \quad (\text{S22})$$

since $K_H = \beta \langle e^{-\beta U} \rangle$ [2]. Thus, the standard entropy change of adsorption for model 0 is:

$$\Delta S^\circ = -R + R \ln \left(\beta P^\circ \frac{\epsilon}{M} \right). \quad (\text{S23})$$

If we plug the expression for the standard entropy change upon adsorption in eqn 23 into Bhatia and Myers’ formula in eqn 20, we arrive at:

$$\Delta H_{opt} = U_{0,opt} - RT = RT \ln \left(\frac{\sqrt{P_L P_H} \epsilon}{RT M} \right) - RT, \quad (\text{S24})$$

which is equivalent to eqn 4 in the main text. This completes our proof of equivalence.

As a second check, we note that our Langmuirian $K := \frac{\beta \epsilon V e^{-\beta U_0}}{M}$ for $U_{0,opt}$ is equal to $\frac{1}{\sqrt{P_L P_H}}$, the optimal Langmuirian constant derived in [14].

S4.4 The density of sites M is important

A material with a suboptimal heat of adsorption can have a much higher deliverable capacity than a material with an optimal heat of adsorption if the latter has a smaller density of sites. See Fig S2 for a sketch to see how two Langmuirian materials that are equally porous, each tuned to have the optimal heat of adsorption, differ in deliverable capacity by a factor of 8!

S5 Model 1 details

S5.1 Derivation

With guest-guest interactions, the total energy U of a system of σ guest molecules adsorbed in the model material is:

$$U = \sigma U_0 + \sum_i \sum_{j>i} z U_{gg} \frac{\sigma}{M} = \sigma U_0 + \frac{1}{2} \sigma z U_{gg} \frac{\sigma}{M}, \quad (\text{S25})$$

¹Note that the units are consistent here because we substituted one unit volume in the Langmuir isotherm expressions for σ

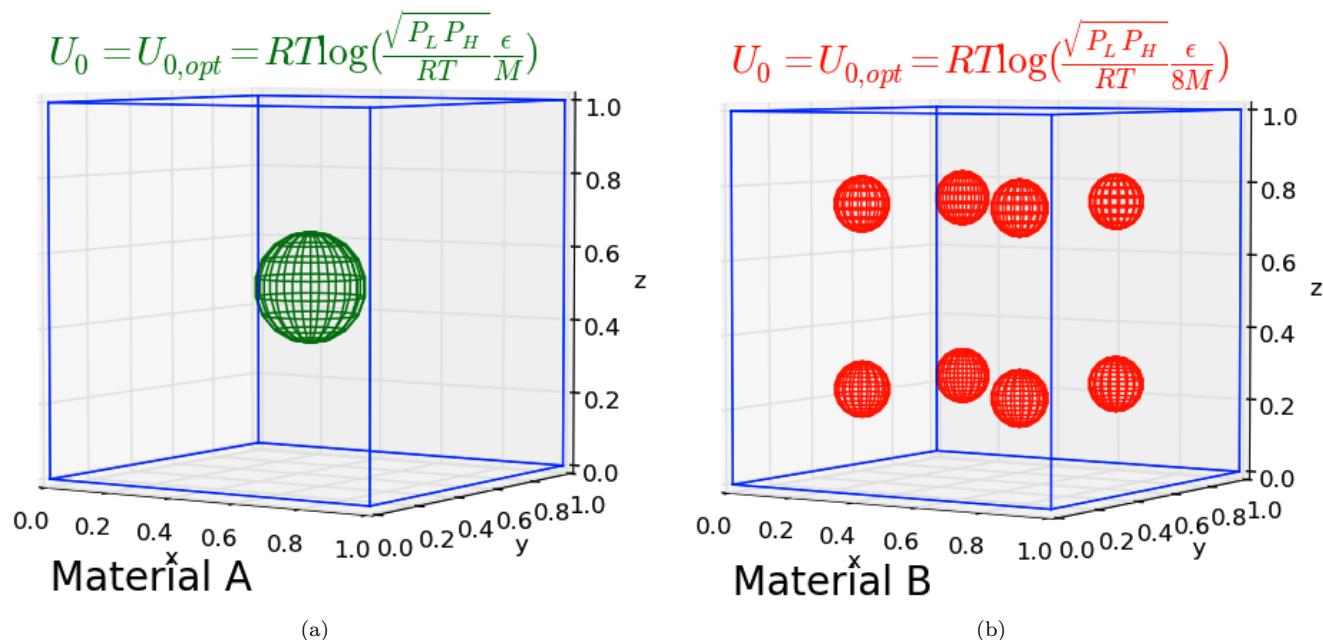


Figure S2. Materials x and y have unit cells, the blue box, of equal sizes. Material A has $M = 1$ sites of radius $2R$, and material B has $8M$ sites of radius R , making them equally porous. Each material has individually tuned heats of adsorption to the optimum, but they differ in deliverable capacity by a factor of 8 because material A has a lower density of sites.

where the first term is the guest-framework interaction energy and the second term is the guest-guest interactions (the factor of $\frac{1}{2}$ avoids over-counting). Now, we write the canonical partition function as:

$$Q(\sigma, M, T) = \frac{M!}{\sigma!(M-\sigma)!} \frac{1}{\Lambda^3} \int_{\Omega} e^{-\beta U} dx_1 dx_2 \cdots dx_{\sigma}. \quad (\text{S26})$$

Using eqn S25 and the void fraction ϵ , we write evaluate the integral to get:

$$Q(\sigma, M, T) = \frac{M!}{\sigma!(M-\sigma)!} \frac{1}{\Lambda^3} \left(\frac{V}{M} \epsilon \right)^{\sigma} e^{-\beta \sigma U_0 - \beta z U_{gg} \frac{\sigma^2}{2M}}. \quad (\text{S27})$$

Following Approach 1 above, we apply Stirling's formula for the factorial terms and take the derivative of the logarithm with respect to σ to get an expression for μ_{ads} and then equate this to μ_{ig} to arrive at:

$$\frac{M-\sigma}{\sigma} \frac{\epsilon V}{M \Lambda^3} e^{-\beta U_0} e^{-\beta z g \sigma / M} = (\Lambda^3 \rho)^{-1}. \quad (\text{S28})$$

In contrast to the Langmuir isotherm derivation, we cannot solve this equation explicitly for σ . However, we gain some intuition by writing this as:

$$\frac{\sigma}{M} = \frac{K e^{-\theta \sigma / M} P}{1 + K e^{-\theta \sigma / M} P}, \quad (\text{S29})$$

where $\theta := \beta U_{gg} z$ is a guest-guest interaction dependent term and $K := \frac{\beta \epsilon V e^{-\beta U_0}}{M}$ as previously.

S5.2 Asymptotic Expansion

To gain insight into how the guest-guest interactions cause a deviation from a Langmuirian curve, we seek to make an approximation to eqn S29 for small θ . We Taylor expand the exponential term in eqn S29 as $e^{-\theta\sigma/M} \approx 1 - \theta\sigma/M$ and get a quadratic equation for $\frac{\sigma}{M}$:

$$KP\theta \left(\frac{\sigma}{M}\right)^2 - (1 + KP(1 + \theta)) \frac{\sigma}{M} + KP = 0. \quad (\text{S30})$$

Next, we seek an asymptotic expansion:

$$\frac{\sigma}{M} \sim \sigma_0 + \theta\sigma_1 + \dots \quad (\text{S31})$$

and substitute this into eqn S30. Equating terms at order 1, we get the Langmuir isotherm at leading order:

$$\sigma_0 = \frac{KP}{1 + KP}, \quad (\text{S32})$$

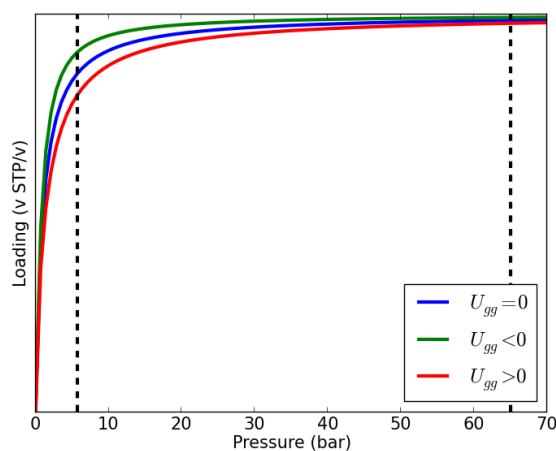
and at order θ we get the correction term:

$$\sigma_1 = \sigma_0^2(\sigma_0 - 1), \quad (\text{S33})$$

which is the expression in eqn 11.

S5.3 How unfavorable guest-guest interactions may enhance a material's deliverable capacity

Fig 3(a) shows an example material with guest-guest interactions turned off, where the isotherm would be described by the Langmuir isotherm (blue curve), as well as when guest-guest interactions are favorable for adsorption (decreasing the energy of the site, $U_{gg} < 0$) and unfavorable (increasing the energy of the site, $U_{gg} > 0$). Using $P_L = 5.8$ bar and $P_H = 65$ bar, we see that the unfavorable guest-guest interactions, in this case, enhance the deliverable capacity because they reduce uptake at P_L more than they reduce uptake at P_H . In contrast to what we found with SBN, here favorable guest-guest interactions erode the deliverable capacity by increasing adsorption at P_L but not at P_H .



(a)

Figure S3. An example of how guest-guest interactions that lower the energy of an adsorption pocket can decrease the deliverable capacity by increasing uptake at P_L more than it increases uptake at P_H . Here, repulsive guest-guest interactions would enhance the deliverable capacity.

S6 Model 2 details

S6.1 Computing the standard entropy change

We use equation S21 to calculate the standard entropy change upon adsorption. The enthalpy change upon adsorption is $\Delta H = \langle U \rangle - RT$. [To help keep track of the signs: $\langle U \rangle$ will be negative for a good material.] The Henry coefficient is computed by $\langle \beta e^{-\beta U} \rangle$. Finally, we get the maximum loading following the method outlined in [13], where we first compute the Helium pore volume V_p :

$$V_p = \int e^{-\beta U_{He-s}} dV, \quad (\text{S34})$$

from Monte Carlo simulation. The term U_{He-s} is the solid-helium interaction energy. In the effective potential in eqn 12, we simply use the helium-methane Lennard-Jones parameters to model helium adsorption. We used a surface density of carbon atoms $\alpha = 0.13 \text{ \AA}^{-2}$. From the Helium pore volume, we estimate the maximum loading by:

$$M = V_p \rho_{CH_4,l}, \quad (\text{S35})$$

where $\rho_{CH_4,l} = 422.62 \text{ kg/m}^3$ is the liquid density of methane.

The fractional deliverable capacity was computed by writing the isotherms for model 2 as:

$$\sigma = \frac{K_H P}{1 + \frac{K_H P}{M}}. \quad (\text{S36})$$

S6.2 More detailed description of the model

The unit cell of the model material in model 2 is assigned a cube with dimension $2R + \sigma_{O-O} 2^{1/6}$, where $\sigma_{O-O} = 3.1 \text{ \AA}$ from the Universal Force Field [15]. We use $\sigma = \sigma_{CH_4-O}$ from [16] for eqn 12, which is the force field used for all zeolite molecular simulations in this work. Choosing this unit cell corresponds to the assumption of spheres packed in a cubic lattice, where the spherical shells, composed of O atoms here, are at their optimal distance apart at most. To be precise, the energy landscape of the material is defined as:

$$U(r) = \begin{cases} U_{eff}(d = R - r), & r < R \\ \infty, & r \geq R. \end{cases} \quad (\text{S37})$$

where $U_{eff}(d)$ is given in the main text eqn 12 from the work in [17].

Using the energy landscape in eqn S37, we perform Widom insertions [2] in Python using the numpy package to get the Henry coefficient K_H from equation S2. For structures with loading greater than 20 v STP/v at 200 bar, we use the saturation loading M computed from the Langmuir fitting routine. For structures with loading less than 20 v STP/v at 200 bar, we assume that the isotherm was not simulated up to a high enough pressure for the Langmuir fitting routine to accurately estimate the saturation loading. Thus, for these structures, we use the void fraction computed from Zeo++ and the liquid density of methane to estimate the max loading M , similar to eqn S35. We sample the energy of adsorption to calculate the ensemble average heat of adsorption $\langle U \rangle$ as well. With K_H and $\langle U \rangle$, we calculate ΔS from eqn S21 and $\Delta H = \langle U \rangle - RT$. This is how Fig 8(d) was generated.

S6.3 Barrier to observed entropy change

The work in [18] intuitively pointed out that there is a bound to the change in entropy that a guest molecule can experience in the framework. In accordance, we see a sharp bound in Fig 8(a). However, there are some outliers that we omitted, and we show them here in Fig S4(a). Fig S4(b) shows that these outliers have a very low void fraction and thus experience the greatest change in entropy upon adsorption (via eqn 23).

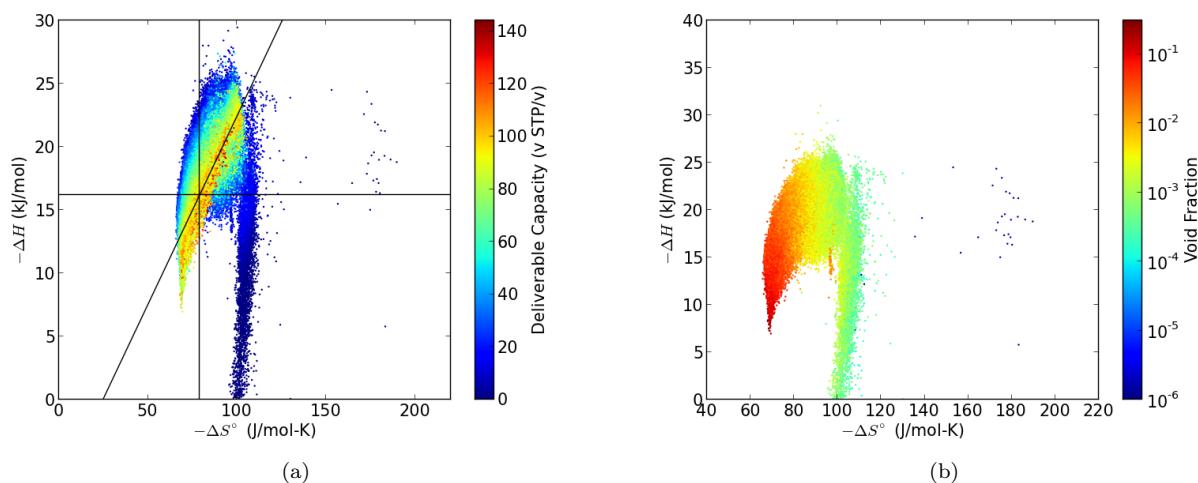


Figure S4. Outliers in the dataset, as they experience entropy changes > 120 J/mol-K. These structures have a very small void fraction, consistent with eqn S23.

S7 Model 3: Spatially inhomogeneous adsorption site

In models 0 and 1, the energy of a guest molecule inside the adsorption site is assumed to be spatially homogeneous. As a consequence, the energy of adsorption in models 0 and 1 does not depend on temperature. If we increase the temperature in a system with a real material, methane will explore higher energy configurations and, as a consequence, the heat of adsorption will increase (become less negative). To include this effect, we consider a spherical adsorption site with a radially symmetric harmonic energy landscape ($r = 0$ is the center of the site with radius r_0 in Fig 3):

$$U(r) = \begin{cases} -U_d + \frac{1}{2}kr^2, & r < r_0 \\ \infty, & r \geq r_0. \end{cases} \quad (\text{S38})$$

As $T \rightarrow 0$, entropy becomes irrelevant and the adsorbed particle resides at the center of the adsorption site $r = 0$. As the temperature increases from zero, entropic considerations take effect, and the guest molecule explores a greater region of the adsorption site, and hence a greater region of the bottom of the harmonic potential in eqn S38. The ensemble average energy of adsorption with the energy landscape in eqn S38 is:

$$-U_d + \frac{3}{2}RT. \quad (\text{S39})$$

The increase with temperature reflects the greater exploration of the trough in the harmonic potential at higher temperatures in the ensemble. If the harmonic potential is steep enough (i.e., sufficiently strong such that the methane remains close to the minimum), we can derive from statistical mechanics an approximate isotherm of the model material in Fig 3 with the energy landscape in eqn S38:

$$\frac{\sigma}{M} = \frac{\beta\Psi e^{\beta U_d} P}{1 + \beta\Psi e^{\beta U_d} P}, \quad (\text{S40})$$

where

$$\Psi := \sqrt{2} \left(\frac{\pi RT}{k} \right)^{\frac{3}{2}}. \quad (\text{S41})$$

Comparing eqn S40 with the Langmuirian isotherm in eqn 2, Ψ is the analogy of $\frac{\epsilon}{M}$ —the volume of an adsorption site—in model 0. As k increases, i.e., as the harmonic potential well becomes steeper, the effective volume per site Ψ decreases.

As the temperature increases, the effective volume per site Ψ increases since an adsorbed guest particle can explore more of the trough for a fixed k . This derivation gives a natural definition for the void fraction of a material with a harmonic potential and shows that the effective volume per adsorption site scales with $T^{\frac{3}{2}}$.

Defining the deliverable capacity with the isotherm in eqn S40 and optimizing with respect to U_d results in:

$$U_{d,opt} = U_{d,opt}(\Psi) = RT \ln \left(\frac{\sqrt{P_L P_H}}{(RT)} \psi \right). \quad (\text{S42})$$

essentially the same as eqn 4. In real materials, whose energy landscape is a more complicated function of space than the prescription in eqn 1, the void fraction is ill-defined without a threshold energy beyond which the framework is deemed as unoccupiable by a guest molecule. Still, the result in eqn S40 suggests that real materials may be analyzed in the context of models 0 and 1, despite the “binding site” region Ω_s depicted in Fig 3 being ambiguous in real materials. i.e., the energy landscape of a real material can be mapped to a void fraction ϵ to be used in eqn 4. For a Harmonic potential, the mapping is $\frac{\epsilon}{M} \rightarrow \Psi$. We found that an energy threshold of $\langle U \rangle + RT$ to determine which points are occupiable for defining the void fraction for Fig 4 provided a reasonable mapping of for the Langmuirian zeolites with an energy landscape defined by a pair-wise Lennard-Jones model.

S7.1 Model 3 derivation

Here we derive the isotherm in eqn S40. The single particle partition function for a single site is:

$$q = \frac{1}{\Lambda^3} \int_{\Omega} e^{\beta U_d - \frac{1}{2} k \beta r^2} dx = \frac{e^{\beta U_d} 4\pi}{\Lambda^3} \int_0^{r_0} r^2 e^{-\frac{1}{2} k \beta r^2} dr. \quad (\text{S43})$$

Next, we rescale the r in the integral above by $\hat{r} := \frac{r}{r_0}$ to get a new integral:

$$\Lambda^3 q = \int_0^1 r_0^3 \hat{r}^2 e^{-\frac{1}{2} k \beta r_0^2 \hat{r}^2} d\hat{r}. \quad (\text{S44})$$

Our approximation is as follows. If $\frac{1}{2} k \beta r_0^2 \gg 1$, the above integration in \hat{r} can be approximated by the same integral from 0 to ∞ since $\int_1^{\infty} (\dots) d\hat{r} \approx 0$. With this approximation, we get:

$$q = \frac{1}{\Lambda^3} 4\pi \sqrt{\frac{\pi}{2}} \left(\frac{RT}{k} \right)^{\frac{3}{2}} e^{\beta U_d}. \quad (\text{S45})$$

In words, the approximation is reasonable if the harmonic potential in eqn S38 is steep in the scaled coordinate \hat{r} . Using this single-particle partition function for constructing the Grand Canonical partition function, the logic starting from eqn S15 follows for deriving $\langle \sigma \rangle$ for the harmonic potential, and we arrive at eqn S40.

The ensemble average heat of adsorption in expression S39 is calculated by the expression:

$$\frac{\int_{\Omega} U e^{-\beta U} dx}{\int_{\Omega} e^{-\beta U} dx}, \quad (\text{S46})$$

and invoking the same approximation above under the assumption $\frac{1}{2} k \beta r_0^2 \gg 1$.

S8 Fitting Isotherm data to a Langmuir model

Here we derive the equations for fitting a Langmuir model to adsorption data. We have N pressure-loading data pairs (P_i, L_i) for $i = 1, \dots, N$ organized into a vector $\mathbf{P}, \mathbf{L} \in \mathbb{R}^N$. We also have the Henry coefficient from molecular simulation.

The model prediction $\mathbf{g} \in \mathbb{R}^N$ is a function of the maximum uptake capacity M since we already have the Henry coefficient K_H from simulation:

$$g_i(M) := \frac{K_H P_i}{1 + \frac{K_H}{M} P_i}. \quad (\text{S47})$$

To find the M in the Langmuir model that fits the data, we solve the nonlinear minimization problem

$$\min_M \frac{1}{2} \|\mathbf{g}(M) - \mathbf{L}\|^2. \quad (\text{S48})$$

The M^* that is the minimizer satisfies

$$A(M^*)^T (\mathbf{g}(M^*) - \mathbf{L}), \quad (\text{S49})$$

where A is the N by 1 Jacobian matrix of \mathbf{g} . We solve the minimization problem using the Gauss-Newton method [19]. We start with a guess M_0 and iterate on M using a search direction p_k :

$$M_{k+1} = M_k + p_k. \quad (\text{S50})$$

The search direction is found by, at each iteration, finding the solution p_k to the linear least squares problem:

$$\min_p \|A(M_k)p - (\mathbf{L} - \mathbf{g}(M_k))\|. \quad (\text{S51})$$

For this, we use the Scipy package in Python. The convergence criterion is that the relative change in the sum of square errors is less than 0.0000001.

The Langmuir constant K is then determined by $K = \frac{K_H}{M}$, where M is found by the above fitting routine.

S9 Software

The Matplotlib package in Python, free and open-source software, was used to make the plots in this paper. VisIt Visualization tool was used to make Fig 7(b).

S10 Discourse on ARPA-E target conditions

The Advanced Research Projects Agency Energy of the US Department of Energy posed the operating conditions of 65 to 5.8 bar for a nanoporous material in a vehicular natural gas fuel tank [20]. Here, we justify their target in contrast to the older DOE target of 35 to 1 bar operating pressures.

Charging pressure P_H

The charging pressure should consider:

(i) the threshold pressure above which a two-stage compressor is insufficient (considering infrastructure costs for refilling stations)

(ii) Tank manufacturing standards– 65 bar is a threshold pressure for cheaper, conformable tanks.

Thus, we use $P_H = 65$ bar for our screening. Note that an adsorbent will certainly store more at 65 bar than 35 bar. If a material is worse off at the 65 - 5.8 bar range, it is because the material takes up a substantial amount of cushion gas at the discharge pressure P_L in comparison to the methane adsorption gained by charging at 65 bar instead of 35 bar.

Discharge pressure P_L

Concerning the discharge pressure, the old DOE condition of using 1 bar seems impractical because there must be a sufficient pressure differential to drive methane flow out of the adsorbent bed and into the engine. The methane flow rate to the engine must be above a threshold value for the car to keep driving.

Choosing a discharge pressure to evaluate an adsorbent depends on the kinetics of methane inside the adsorbent, the surface area of the bed, the size of the pipes from the tank to the engine, the distance of the tank from the engine, the required flow rate, etc. There may be some engineering solutions to allow the adsorbent to reach further depletion before there is an insufficient flow rate to the engine. The discharge pressure of 5.8 bar is thus debatable to an engineer, but for now, however, 1 bar seems too impractical, so we chose 5.8 bar for our meta-screening.

S11 Distributions of properties in the zeolite data base

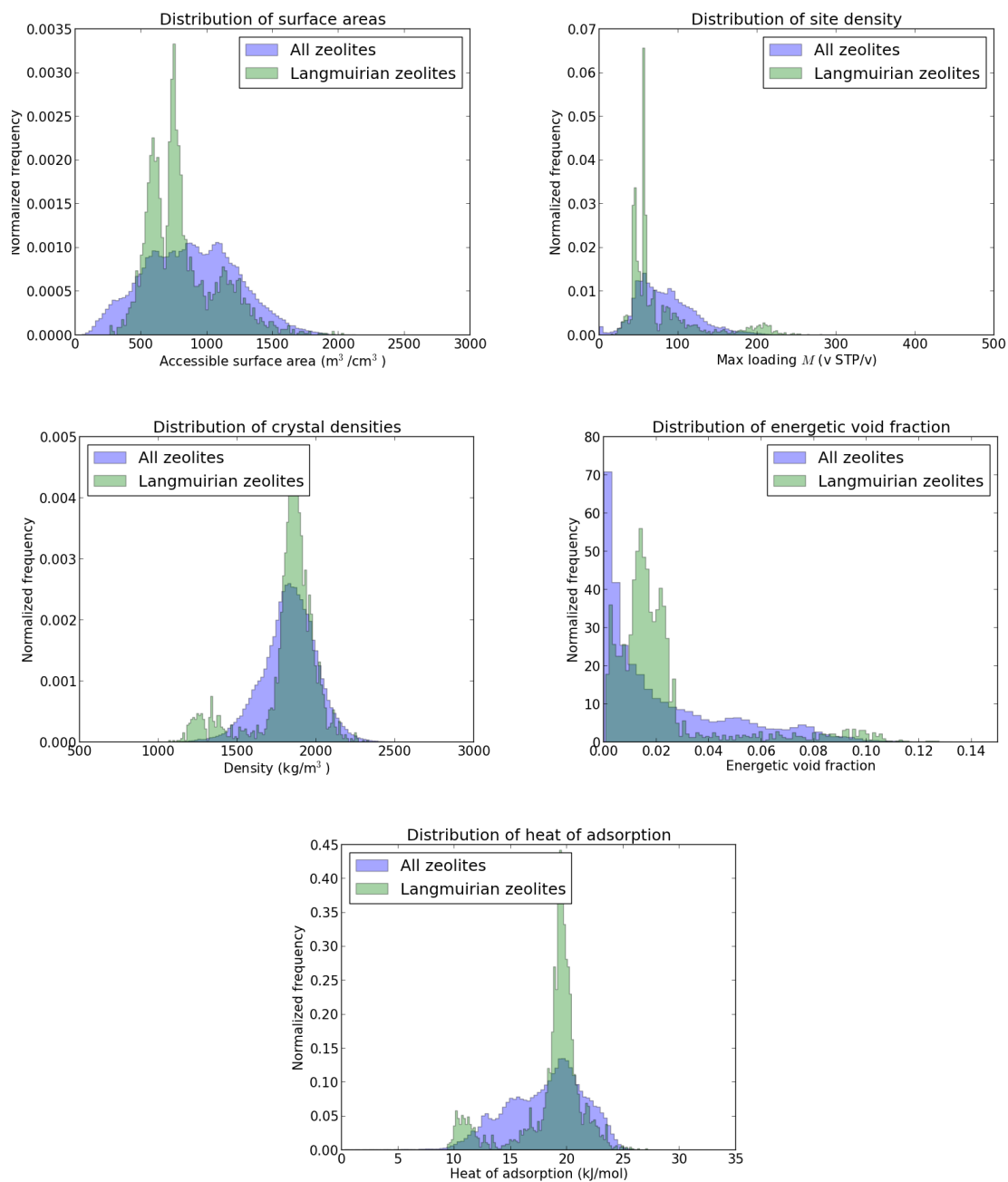


Figure S5. Here, we present probability distributions of different properties of the hypothetical zeolite structures in the SLC database [21] analyzed in this work (those with pore size accessible to methane). For comparison, we also show the distribution for the materials that have the best fit to the Langmuir isotherm in our data fitting routine. These materials were analyzed in the context of model 0. We see that these Langmuirian materials explore a range of these properties, and are thus a diverse set for the analysis.

S12 Other plots of data from the zeolite database

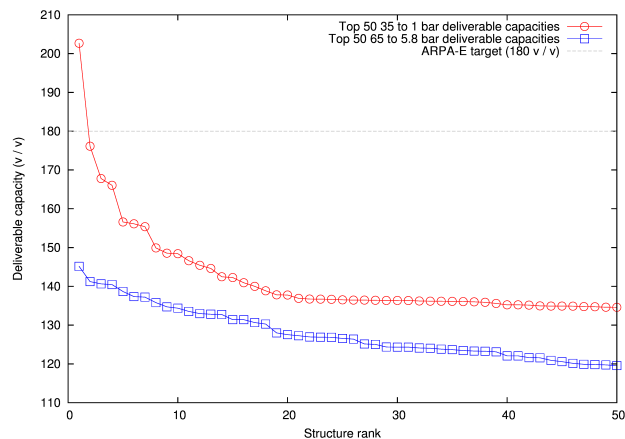


Figure S6. Ranking of hypothetical zeolites with the top deliverable capacities in both the 65 vs 5.8 bar and 35 vs 1 bar pressure range. We see that the two outliers in the 35 vs 1 bar pressure range are the zeolites PCOD8124791 and PCOD8330975 discussed in the main text.

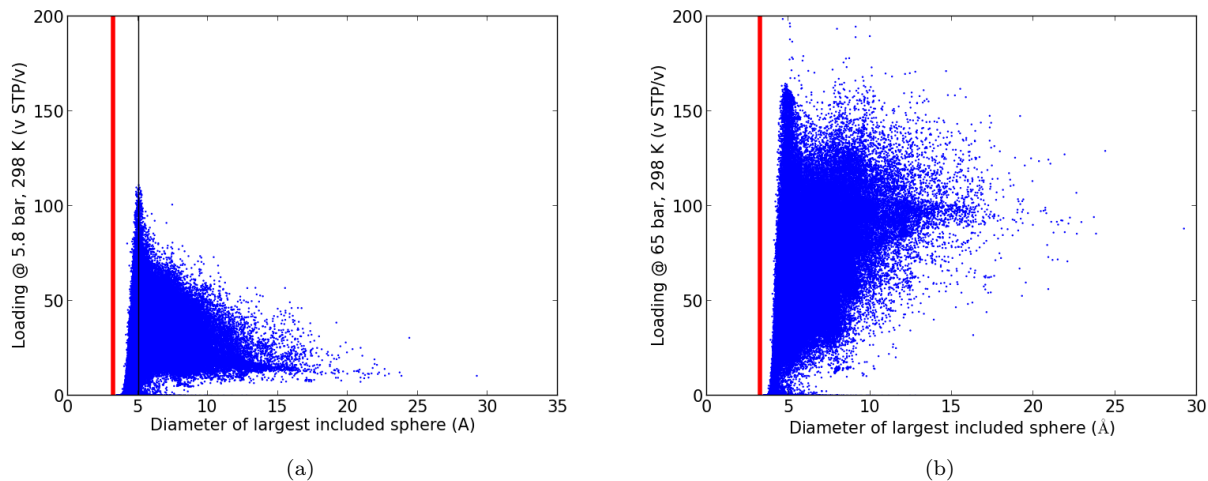


Figure S7. (Top row) Loading at 5.8 bar (a) and 65 bar plotted against the largest included sphere diameter. Red vertical line is hard-sphere diameter of methane. Black vertical lines denote (a) 5.1 Å (b) 4.8 Å.

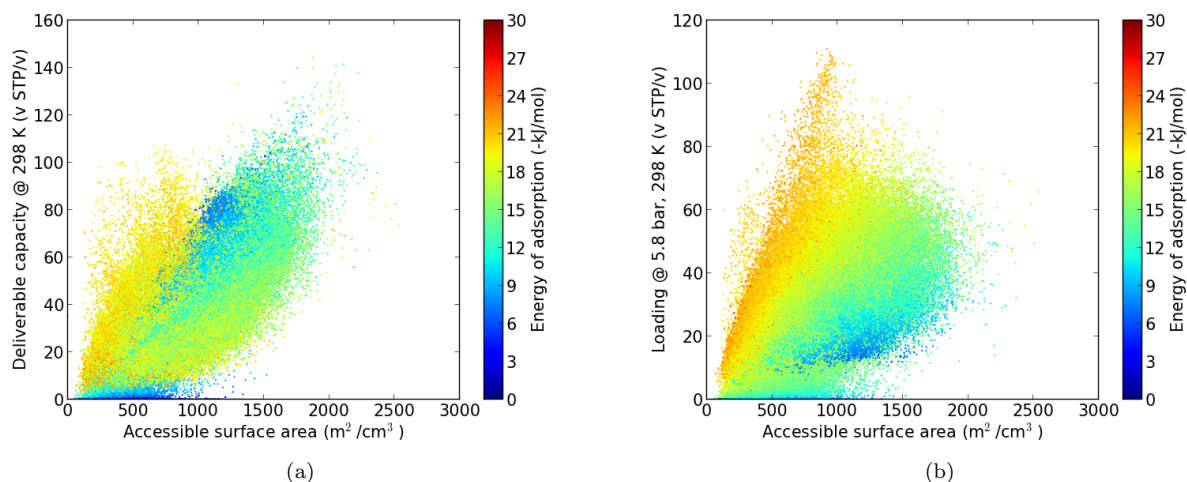


Figure S8. Deliverable capacity (a) and loading at 5.8 bar (b) plotted against accessible surface area. We still see a positive correlation between surface area and deliverable capacity, but the heat of desorption actually decreases the deliverable capacity at high surface areas, unlike what is seen in the loading correlations.

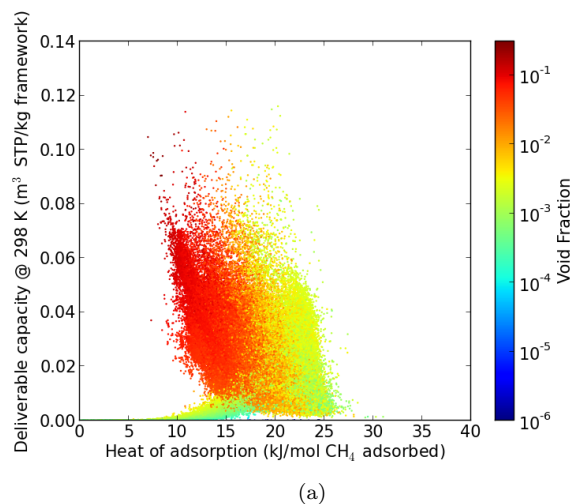
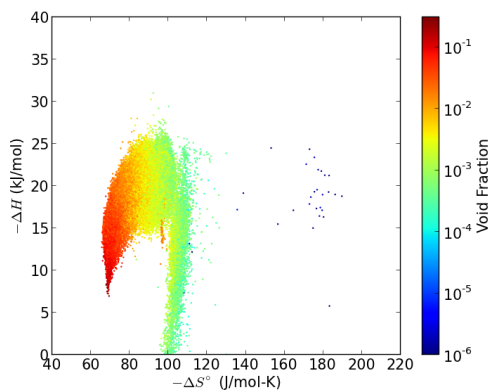
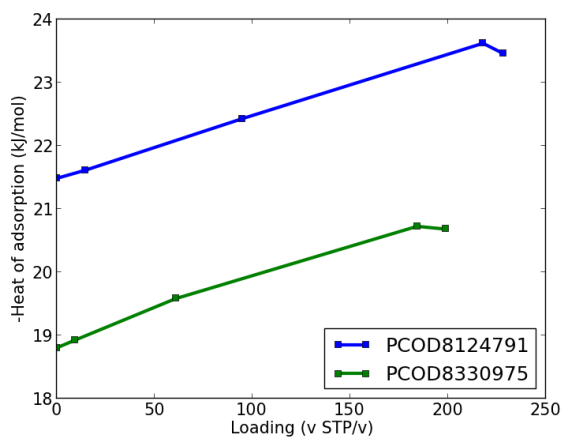


Figure S9. Gravimetric deliverable capacity against energy of desorption color-coded according to the void fraction. For comparison, ARPA-E has a target of $0.5 \text{ g CH}_4/\text{g sorbent} = 0.69 \text{ m}^3 \text{ STP}/\text{kg sorbent}$ to avoid massive tanks. The zeolites thus do not store a high amount of methane per mass.



(a)

Figure S10. Entropy-enthalpy correlation color coded according to the void fraction to corroborate our derivation that the entropy change upon adsorption is related to the void fraction.



(a)

Figure S11. The top two performing 35 to 1 bar deliverable capacity zeolites have heats of adsorption that increase with loading, suggesting that attractive guest-guest interactions are present.

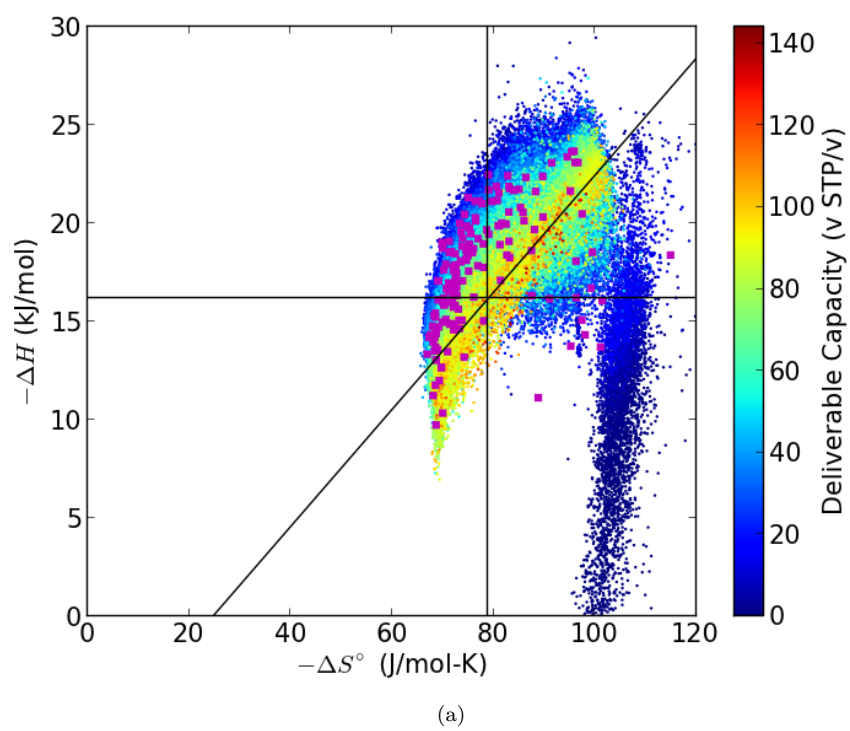


Figure S12. The IZA zeolite structures are plotted as pink points in $(\Delta S^\circ, \Delta H)$ space for comparison with the hypothetical zeolites.

References

1. J. Kim and B. Smit. Efficient monte carlo simulations of gas molecules inside porous materials. *Journal of Chemical Theory and Computation*, 8(7):2336–2343, 2012.
2. D Frenkel and B Smit. *Understanding molecular simulation: From algorithms to applications*. 1996.
3. D Dubbeldam, S Calero, TJH Vlugt, R Krishna, Th LM Maesen, E Beerdsen, and B Smit. Force field parametrization through fitting on inflection points in isotherms. *Physical review letters*, 93(8):088302, 2004.
4. Sofia Calero, David Dubbeldam, Rajamani Krishna, Berend Smit, Thijs JH Vlugt, Joeri FM Denayer, Johan A Martens, and Theo LM Maesen. Understanding the role of sodium during adsorption: A force field for alkanes in sodium-exchanged faujasites. *Journal of the American Chemical Society*, 126(36):11377–11386, 2004.
5. Berend Smit and Theo LM Maesen. Towards a molecular understanding of shape selectivity. *Nature*, 451(7179):671–678, 2008.
6. Berend Smit and Theo LM Maesen. Molecular simulations of zeolites: Adsorption, diffusion, and shape selectivity. *Chemical reviews*, 108(10):4125–4184, 2008.
7. Matthew S Sun, DB Shah, Heather H Xu, and Orhan Talu. Adsorption equilibria of c1 to c4 alkanes, co2, and sf6 on silicalite. *The Journal of Physical Chemistry B*, 102(8):1466–1473, 1998.
8. W Zhu, F Kapteijn, and JA Moulijn. Adsorption of light alkanes on silicalite-1: Reconciliation of experimental data and molecular simulations. *Physical Chemistry Chemical Physics*, 2(9):1989–1995, 2000.
9. C Martin, N Tosi-Pellenq, J Patarin, and JP Coulomb. Sorption properties of alpo4-5 and sapo-5 zeolite-like materials. *Langmuir*, 14(7):1774–1778, 1998.
10. E Beerdsen and B Smit. Diffusion in confinement: Agreement between experiments better than expected. *The Journal of Physical Chemistry B*, 110(30):14529–14530, 2006.
11. Thomas F. Willems, Chris H. Rycroft, Michael Kazi, Juan C. Meza, and Maciej Haranczyk. Algorithms and tools for high-throughput geometry-based analysis of crystalline porous materials. *Micropor. Mesopor. Mat.*, 149(1):134 – 141, 2012.
12. Suresh K. Bhatia and Alan L. Myers. Optimum conditions for adsorptive storage. *Langmuir*, 22(4):1688–1700, 2006.
13. Alan L. Myers. Characterization of nanopores by standard enthalpy and entropy of adsorption of probe molecules. *Colloids Surf. A*, 241(13):9 – 14, 2004. Proceedings of the Third International TRI/Princeton Workshop, Characterization of Porous Materials: from Angstroms to Millimeters.
14. Kimberly R. Matranga, Alan L. Myers, and Eduardo D. Glandt. Storage of natural gas by adsorption on activated carbon. *Chem. Eng. Sci.*, 47(7):1569 – 1579, 1992.
15. A. K. Rappe, C. J. Casewit, K. S. Colwell, W. A. Goddard, and W. M. Skiff. Uff, a full periodic table force field for molecular mechanics and molecular dynamics simulations. *J. Am. Chem. Soc.*, 114(25):10024–10035, 1992.
16. E. García-Pérez, J.B. Parra, C.O. Ania, A. García-Sánchez, J.M. Baten, R. Krishna, D. Dubbeldam, and S. Calero. A computational study of co2, n2, and ch4 adsorption in zeolites. *Adsorption*, 13(5-6):469–476, 2007.
17. J.A. Ripmeester and CI Ratcliffe. Application of xenon-129 nmr to the study of microporous solids. *J. Phys. Chem.*, 94(19):7652–7656, 1990.

18. E. Garrone, B. Bonelli, and C. Otero Aren. Enthalpy-entropy correlation for hydrogen adsorption on zeolites. *Chem. Phys. Lett.*, 456(13):68 – 70, 2008.
19. U. Ascher and C. Greif. *A first course in numerical methods*. 2011.
20. Methane opportunities for vehicular energy (move). funding opportunity announcement. pages <http://arpa-e.energy.gov/?q=arpa-e-site-page/view-programs>, Advanced Research Projects Agency - Energy, US Department of Energy, 2012.
21. Ramdas Pophale, Phillip A. Cheeseman, and Michael W. Deem. A database of new zeolite-like materials. *Phys. Chem. Chem. Phys.*, 13:12407–12412, 2011.